

CESR-c Status and Accelerator Physics

D. Rice

LEPP-Cornell Univ., Ithaca, NY 14853 USA

The CESR-c/CLEO-c project at the Laboratory for Elementary-Particle Physics will provide a timely increase of 2 orders of magnitude in world D and D_s data samples, and an order of magnitude in $\psi(3100)$ decays. Providing the requisite luminosity in a collider designed for 8 GeV per beam will be facilitated with enhancement of radiation damping by strong wiggler magnets. These wigglers will be emitting 90% of the beams' synchrotron radiation power. In preparation for operation in this lower energy regime we have studied several accelerator physics topics that may affect operation. We present some results herein.

1. INTRODUCTION

1.1. The Cornell Electron Storage Ring

CESR has operated since 1978 primarily for the study of B decays in the 4.7-5.6 GeV beam energy range. Throughout the past 2 decades multiple machine upgrades have increased the peak luminosity to above $1 \times 10^{33} \text{ cm}^{-2}\text{-sec}^{-1}$ [1,2,3].

A unique and critical feature of CESR is the support of many bunches in each beam counter rotating in a single vacuum chamber. [3] The large closed orbit distortion ("pretzel") used to separate the beams at parasitic crossing points exacerbates the effects of multipole fields through feed down, creating special demands on field quality. These pretzel orbits are approximately equal and opposite displacements for each beam. The long range beam-beam interaction at the 89 potential parasitic crossing points restricts aperture and causes current dependent closed orbit distortions and tune shifts varying from one bunch to another.

Fully independent control of all quadrupole and sextupole strengths gives the maximum possible flexibility in optics design and correction. This feature has proven essential to compensate the effects of the large pretzel orbit and strong wiggler magnets.

Fast injection is provided by a linac and synchrotron, the latter being of comparable circumference as the storage ring. This feature permits full energy, multiple (limited by beam loading in the linac and converter power) bunch injection into CESR, enabling filling times as little as 5 minutes.

1.2. CESR-c Objectives

The adaptability of the CESR facility combined with the capability and B physics experience of the CLEO detector provide a facility ideally suited to make a significant contribution to physics at the charm threshold. [4] We expect to increase the sample of D and D_s decays by two orders of magnitude in 3 years of running. The CLEO detector's tracking and photon resolution, large solid angle, particle identification, and trigger flexibility place it well to carry out this study.

In order to provide the particle decays for the CLEO-c program, CESR must reach luminosities well into the $10^{32} \text{ cm}^{-2}\text{-sec}^{-1}$ regime, delivering yearly integrated luminosity on the order of 1-2 fb^{-1} . While this

luminosity is modest compared to the $1.3 \times 10^{33} \text{ cm}^{-2}\text{-sec}^{-1}$ achieved by CESR at 5.3 GeV, the reduced damping and increased sensitivity to perturbations at the lower energy will provide challenges in accelerator physics and operation. Though much work will go toward optimizing performance between 1.5 and 2.5 GeV beam energy, the capability of $10^{33} \text{ cm}^{-2}\text{-sec}^{-1}$ operation at 5.3 GeV will be preserved.

1.3. CESR-c Challenges

At 2 GeV CESR-c will be operating at only 25% of the initial design energy of 8 GeV. Compared to 5.3 GeV, at 1.9 GeV the synchrotron radiation decreases by a factor of 60 and the damping time increases by a factor of 22. The decrease in beam rigidity of ± 2.5 adds another level of tenderness to the beam. To counter these effects we are improving control of field errors and instability driving mechanisms, and enhancing radiation damping with 15.6 m of 2.1 T wigglers. These will place CESR-c outside of the normal operating envelope for colliders in that 90% of the synchrotron radiation will be coming from localized wigglers.

The non-linear particle dynamics, with combined effects from wigglers and the beam-beam interaction, will be exploring a new regime of colliding beam accelerator physics. In addition the effects of long range beam-beam interactions from up to 89 parasitic crossings will be augmented at the lower energy. Effects from the parasitic crossings include bunch-by-bunch and current dependent closed orbit distortions and tune shifts, as well as a nearly hard-edge aperture restriction for the beams.

Other, more predictable, accelerator physics effects such as bunch lengthening, Touschek scattering, lifetime from gas scattering, have been calculated and experimentally verified to be acceptable for CESR-c operation.

1.4. Modifications for CESR-c

The following modifications are being made to CESR to optimize performance in the 1.5-2.5 GeV energy range:

- Restore radiation damping lost at low energy with ~ 16 m of 2.1 T wigglers
- Replace thick Ti windows with Be windows in injection transfer lines

- Modifications to power supplies to reduce ripple and resulting tune modulation on beams
- Reduce β_v^* from 1.8 to 1 cm
- Reduce bunch length to 1 cm by increasing the peak accelerating gradient in 4 single cell superconducting RF cavities to 10 MV/m (2.5 MV/cell)

The reduction of β_v^* and increase in RF cavity gradient have been planned for 5.3 GeV operation. The construction and installation of wiggler magnets is the only major upgrade required for CESR-c operation.

2. CESR-C WIGGLER MAGNETS

2.1. Choosing Wiggler Parameters

The energy scaling of beam parameters with bending magnet dominated radiation may be altered by adding wiggler magnets to the ring. When wiggler radiation dominates in a ring the scaling of critical parameters with wiggler parameters is:

$$\begin{aligned} \text{Damping time:} & \quad \tau \propto \frac{1}{L_w B_w^2} \\ \text{Horizontal Emittance:} & \quad \epsilon_x \propto B_w H_w \\ \text{Energy Spread:} & \quad \frac{\sigma_E}{E_0} \propto \sqrt{B_w} \end{aligned}$$

where B_w is the peak wiggler field, L_w the total length of wigglers, and H_w the emittance parameter at the wiggler.

From these equations we can see that the beam energy spread is independent of optics and length of wigglers. Thus the maximum acceptable energy spread will determine the peak field in the wigglers. Once this is chosen the damping time will be determined by the length of wigglers in the ring. Finally, the beam emittance is controlled as usual, but with leverage from the wigglers, by tailoring the optics functions.

While several potential technologies for the wigglers were explored, the peak field of 2.1 T and the need to preserve a ± 2.5 cm vertical beam aperture quickly narrowed the candidates to those employing superconducting technology. Superferric construction using NbTi wire was chosen.

2.2. Magnetic Design

With the introduction of strong wigglers into the storage ring lattice, the effects on optics must be carefully considered. Even a perfect wiggler, with purely sinusoidal $B_y(z)$ and infinitely wide poles (no $B_y(x)$ variation) exhibits strong focusing only in the vertical plane.[5] (Coordinate convention is z for beam direction, y vertical, and x horizontal or radial.) The equation below gives the integral of the vertically deflecting field (labeled B_x) along the beam path of an ideal wiggler.

$$\int_{\text{wiggler}} B_x ds = -\frac{L_w B_w^2}{2B\rho} \left(y + \frac{2}{3} k_w^2 y^3 + \dots \right) \quad (k_w = 2\pi/\lambda_w)$$

It is important to note that the subscript x of B is with respect to the instantaneous path of the beam through the wiggler, not the laboratory frame. From the equation above it is clear that all the vertical focusing terms increase as B_w^2 and the non-linear terms (only the first, cubic nonlinearity, is shown) are also dependent on the period of the wiggler. Each of the 1.3 m long wigglers in CESR-c changes increases the vertical tune by about 0.1 integer. The period of the wigglers should be as long as possible to minimize the effects of this cubic nonlinearity.

However, these considerations hold only for ideal wigglers. Realistic dimensions result in a variation of $B_y(x)$. Although this variation may be symmetric about the centerline and have no net contribution to a straight-line integral through the magnet, the beam samples this changing field periodically, resulting in significant effects on beam dynamics. An approximation for the effect of a changing field is given by: [6]

$$\int_{\text{wiggler}} B_y ds \approx -\frac{1}{2} L_w A_x \frac{dB_y}{dx} \quad A_x = \frac{B_w \lambda_w^2}{4\pi^2 B\rho}$$

Here again this effect will be proportional to B_w^2 (assuming dB_y/dx is proportional to B_w). However, it varies directly as λ_w^2 , not inversely. Thus the wiggler period must be chosen as a compromise between these two effects. Parameters of the CESR-c wigglers are given in Table 1 below.

Table 1: CESR-c wiggler specifications

Parameter	Value
Peak field	2.1 T
Pole period	40 cm
Length	1.3 m
Total in CESR	12
Number of poles	8
Technology	Superferric
Pole-to-pole gap	7.6 cm
Field uniformity $\Delta x = \pm 4$ cm	+0, -0.3%
Conductor	0.8 mm NbTi
Cu:SC	1.3:1
Operating margin	50%

During the design and prototype construction the issue of seven vs eight poles was discussed extensively. While arguments may be made for each option, the improved uniformity with excitation and slightly improved symmetry of the transfer function of the eight pole design tilted the decision in its direction. [7] Transfer functions in the horizontal plane (x' out vs x in) are shown for seven and eight pole wigglers both at the central design field (1.9 T) and maximum design field (2.1 T) in Figure 1 below. The transfer functions were

obtained by tracking through field calculated by the 3-D FEA program, TOSCA.

The field uniformity figure of 0.3% drop at ± 4 cm was determined by beam dynamic aperture tracking.

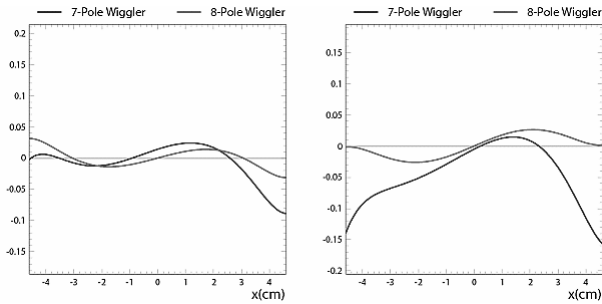


Figure 1: Horizontal transfer functions through wigglers. Blue curves for 7 pole, red for 8 pole wigglers. The left plot is at central (optimum) design field, the right at maximum (and most likely used) design field.

2.3. Wiggler Production and Testing

The wigglers were constructed largely in-house to maintain schedule and quality control. Production details are given in reference [8].

A critical step in fabrication of the wigglers is the final testing and field mapping. This is done in several steps. After checking out all cryogenic systems, the wiggler is trained to about 108% of operating current while logging coil voltages during quenches for future reference. Then two types of magnetic measurements are made. A precision Hall effect probe measuring B_y is moved longitudinally (z direction) through the wiggler, repeating the scans at several displacements in x . This gives point-by-point data useful in localizing any field anomalies. Next a flip coil measurement of the straight-line integral B_y and B_x fields is made at several displacements of the coil center. Both Hall and flip coil measurements are usually repeated at lower currents.

While the flip coil measures along a straight line integral, oblivious to many effects the beam is seeing, it is quite sensitive to construction errors. Small residual first and second integral values (second integral is measured by twisting one end of the pickup coil $\frac{1}{2}$ turn) are measured on some units. Of more concern is a skew field component seen on several magnets - the a_1 (skew quad) component reached as high as 2 G-m/cm. This was found to be caused by accumulation of the effects of sub-mm differences in coil package extension. This has been tentatively fixed by carefully measuring individual coils and balancing their effects within a wiggler (c.f. wiggler #12 in figure 2).

3. CESR-C OPTICS

3.1. Accommodating Wigglers

The vertical focusing of the wigglers must be considered in first order optics design. In fact, separate optics are required for each combination of active wigglers since

turning one off is somewhat like turning off a CESR quadrupole. The nonlinear transfer functions, such as

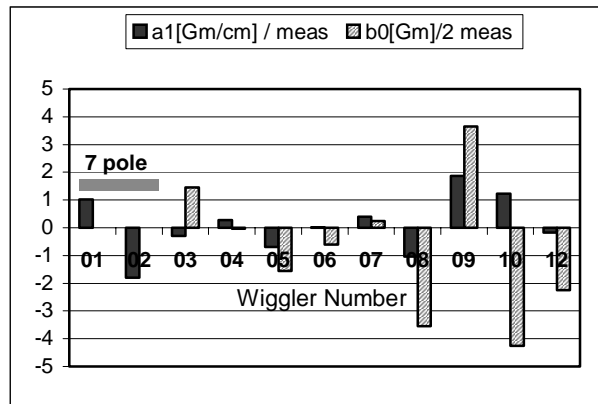


Figure 2: Wiggler dipole error (± 2) and skew quad components for several wigglers.

shown in Fig. 1, feed down into quadrupole and sextupole components at the pretzeled beam position.

In order to accommodate the wigglers in the lattice, their transfer function must be accurately known. Since the lattice design process [9] at CESR involves computation of a matrix of partial derivatives of machine functions, many tracking runs through the arc are required. A quickly evaluated description of the wiggler is essential. Runge-Kutta integration suffers from lack of symplecticity, and symplectic integration techniques are accurate but slow. After extensive work with choices of basis vectors, a 5th order Taylor map (expanded in Cartesian coordinates) is used for optics design, and a 7th order map for dynamic aperture tracking.

3.2. Accommodating Pretzel Orbits

The pretzel orbit used to provide separation between electrons and positrons at parasitic crossings creates two separate machines for the two beams. Each sextupole contributes opposite signed gradients to the two beams, the difference being proportional to sextupole strength times horizontal separation of the beams. Skew quad fields create differential vertical orbit kicks and different vertical orbits through sextupoles create differences in x - y coupling. The nonlinear transfer functions of the wigglers further complicate the optics scene.

Creating optics for pretzeled CESR requires optimizing two machines simultaneously - one for electrons, one for positrons. Independent control of all quadrupoles and sextupoles is essential. This optimization is nontrivial and requires skilled tuning of weights and initial conditions by an expert.

3.3. Dynamic Aperture

Optics are evaluated for dynamic aperture using a 7th order Taylor map for the wigglers, and full description of the rest of the ring including RF cavities. Full pretzel

orbits and parasitic beam-beam interactions are routinely added.

Because the pretzel orbit severely limits the horizontal aperture, all dynamic aperture evaluation is done with actual physical apertures. This results in apertures always less than the physical aperture, so the acceptability of the dynamic aperture is judged by proximity of the calculated aperture limit to critical lifetime contours.

The calculated dynamic aperture (for the current 6 wiggler configuration) is shown in Figure 3. The left plot is without pretzel orbits, the right plot is with design pretzel orbits (positrons). The reduction in aperture when the pretzel is turned on is primarily physical, as suggested by the more or less square profile of the aperture limits. The three quarter-circle reference curves in the lower left corner show 5 hour lifetime contours for $dE = 0, 2,$ and $4 \sigma_E$. Experiments (done at 5.3 GeV) have confirmed the calculations, showing poor beam lifetime when the calculated profiles touch the appropriate reference profiles.

Dynamic aperture performance is critically dependent on sextupole distribution and must be reevaluated whenever changes in linear or non-linear optics are made.

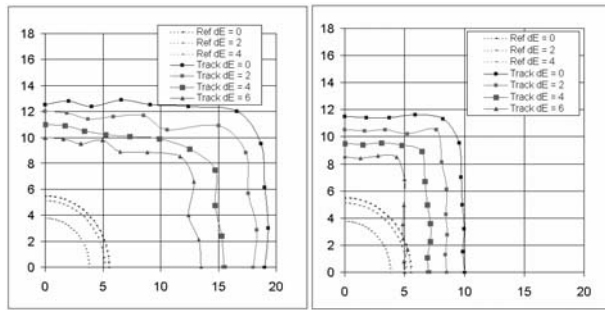


Figure 3: Calculated dynamic aperture without (left) and with (right) orbit-separation pretzel. Scales are labeled in fully coupled (vertical) or uncoupled (horizontal)

beam sigma. The quarter circle reference arcs represent contours for 5 hour lifetime at first 3 energy amplitudes.

4. MACHINE MEASUREMENTS

Six wigglers were installed in CESR during the summer of 2003 - four 8-pole, and two 7-pole assemblies. All were installed in one sector of the accelerator ring to simplify the distribution of cryogenes. The 6 wigglers radiate 80% of the total synchrotron radiation power in the ring and contribute over half of the nonlinearities present in the final CESR-c configuration, giving an excellent test bed to explore the accelerator physics and engineering aspects of low energy operation.

4.1. Wiggler Fields

First priority in machine studies programs went to confirmation of the wigglers' effects on the beam. The most sensitive probe of the wiggler fields is a measurement of betatron tune of the beam as a function of position in the wiggler. Predictions can be made using the wiggler transfer maps and local optics functions at the wigglers. The beam is moved in the wigglers using a local orbit bump. The residual effects of the bump can be checked in conditions where the wigglers are off, but these were found to be small and were not subtracted from the wiggler-on measurements.

The results of a set of such measurements made on a 7 pole wiggler in CESR are shown in Figure 4 below. The left-hand plot shows vertical tune vs. vertical position in the wiggler. The cubic (octupole-like) term is clearly dominant. The center and right-hand plots show horizontal characteristics of the wiggler. These effects are due to the field non-uniformities across the poles, and thus reflect the characteristics of this particular wiggler design (plus construction errors). The added nonlinearities at 2.1 T compared to the central design operating point of 1.9 T are evident.

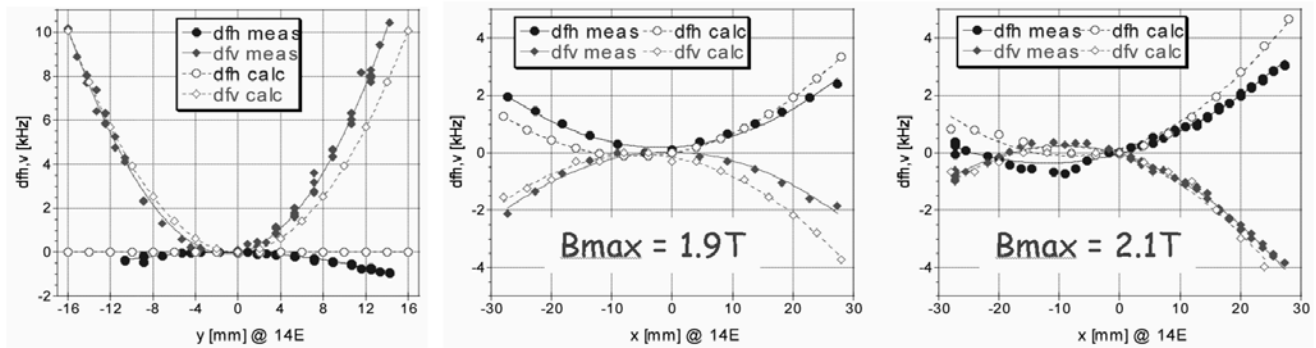


Figure 4: Betatron tune shift vs. position in wiggler - a comparison of measurement with calculation Left hand plot is vertical tune vs. vertical position, center and right hand plots are horizontal.

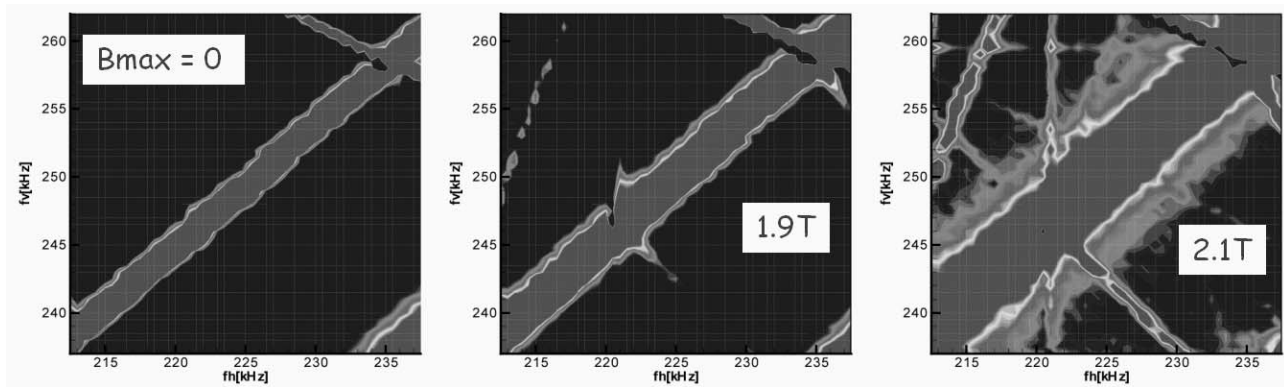


Figure 5: Vertical beam size vs. betatron tunes. Left plot - no wiggler, Center plot - wiggler on at central design field, Right plot - wiggler at maximum design field.

Observation of coupling resonances by measuring vertical beam height as a function of betatron tunes has proven very useful in assessing the non-linear properties of the wigglers. Figure 5 shows several such tune plane scans with the vertical beam size indicated by shades/colors. Resonance lines (Fig. 6) are clearly visible, with a small increase turning on the wiggler to optimum design field, then a more dramatic increase in going to maximum design field. With the wiggler on the following resonances can be seen:

$$\begin{array}{ll}
 -3f_H + f_V = -f_0 & 4f_H + f_V = 3f_0 \\
 -f_H + f_V - f_S = 0 & 2f_H + f_V + 2f_S = 2f_0 \\
 3f_V = 2f_0 & 2f_H - 2f_S = f_0 \\
 f_H + 2f_V + 2f_S = 2f_0 & -3f_H + f_V + f_S = -f_0
 \end{array}$$

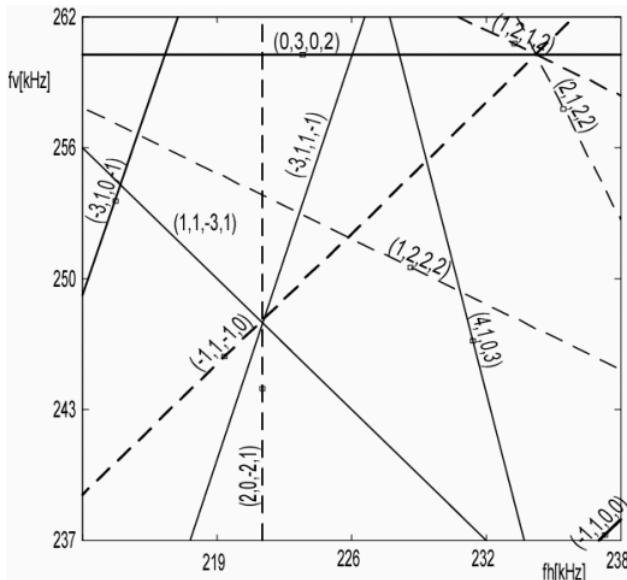


Figure 6: Resonance lines identified in Figure 4. Labels are in order (H,V,S,n)

The field harmonic components responsible for the resonances may be deduced from the resonance orders. Note that without the wiggler the maximum resonance order is 3.

4.2. Bunch Length and Energy Spread

Maintaining a short bunch length to minimize hourglass effects in the beam-beam interaction is critical to CESR-c performance. Measurements of bunch length vs. bunch charge (Fig. 7) show that inductive bunch lengthening is minimal, corresponding to a $Z/n = 0.22 \Omega$, and there is no

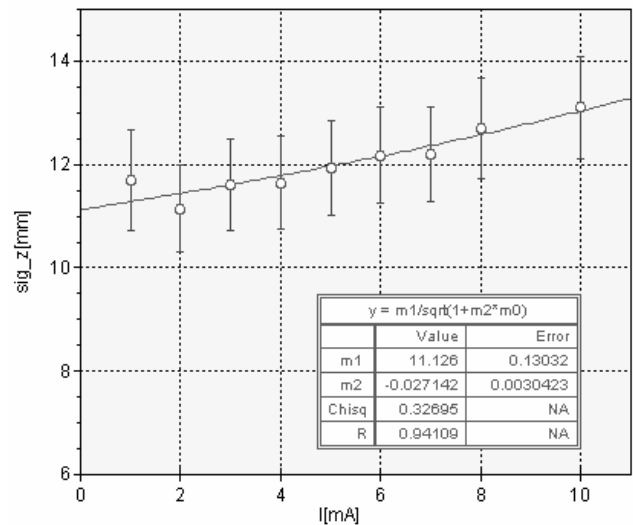


Figure 7: Bunch length measured with a streak camera in CESR at 1.843 GeV with 6 wiggler magnets active.

obvious sign of a microwave threshold at currents more than twice CESR-c design. The zero current bunch length is consistent with expected values.

A related parameter is the beam energy spread. This has been measured by scanning the beam energy across the narrow $\psi(2S)$ resonance and unfolding the beam energy spread from the hadronic cross section momentum width. The measurement gave an energy spread high by one sigma (statistical) of the hadronic cross section measurement.

4.3. Single Beam Instability Thresholds

Thresholds for single beam instabilities should scale as $E_{beam}/(\text{Damping Time})$ for constant effective impedance.

Thresholds for a coupled bunch longitudinal instability were measured under the varying conditions shown below.

Table 1: Longitudinal multi-bunch instability thresholds

Energy (GeV)	Num. Wigglers	τ_E (ms)	I_{thresh} (meas)	I_{thresh} (scaled)
5.3	0	11.4	130 mA	130 mA
4.2	0	24	40 mA	49 mA
1.88	0	255	3 mA	2 mA
1.88	1	110	10 mA	5 mA
1.88	6	45	35 mA	12 mA

The “scaled” thresholds are found by the scaling rule above (reference 5.3 GeV measurement). The measured values (all without active feedback) exceed the scaled by a substantial factor at low energy - particularly as wigglers are turned on. This is likely due to the increased energy spread and dispersive damping from nonlinearities in longitudinal fields, though we do not have a quantitative explanation at this time. The beam energy spread (and bunch length for fixed RF field) increases by a factor of 3.5 when wigglers are turned on.

4.4. Parasitic Crossing Effects

The 89 parasitic crossings, described above, are important in determining performance limits, particularly at lower beam energy. Coherent bunch-by-bunch tune shifts and closed orbit deflections are one aspect of these interactions, and are easily calculated. A more subtle effect is the interaction of bunches with large amplitude particles in the opposing beam, leading to lifetime limits.

In order to gather information on which parasitic crossings are problematic, we can measure bunch-by-bunch loss rates under the influence of a limited number of perturbing counter-rotating bunches.

To make this measurement, all potential bunch positions in one beam are filled with a small (~ 1 mA $\approx 1.6E10$ electrons) charge except the bunches that would collide with the perturbing bunch we wish to fill in the opposing beam. With this configuration the first beam will see parasitic interactions at all except the primary interaction point (or other parasitic interaction points we may optionally wish to exclude from the measurement).

The perturbing bunch (or bunches) in the opposing beam are then filled with successively higher currents until the lifetime of the test beam bunches is reduced. Knowing where the parasitic collisions with the lossy bunches are taking place can then lead to understanding what parameters are critical. The results of such a measurement are shown in Figure 8.

5. LUMINOSITY PERFORMANCE

To date six out of 12 wigglers have been installed, and three months of low energy operation has taken place with roughly 50% of the time in machine studies. Peak luminosity has exceeded $4.5 \times 10^{31} \text{ cm}^{-2}\text{-sec}^{-1}$. The

luminosity performance is consistent with the expected commissioning profile.

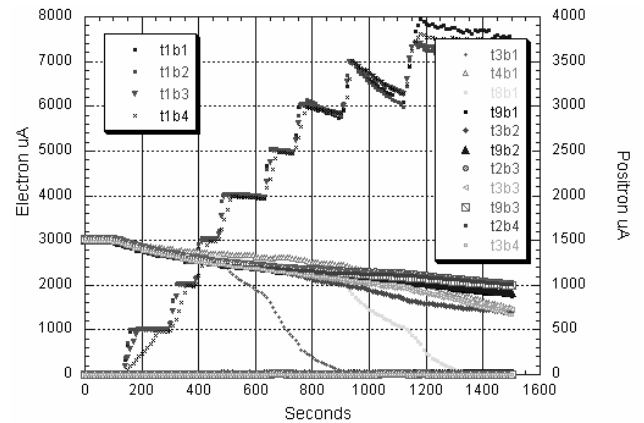


Figure 8: Beam losses from parasitic beam-beam effects. Beam current in strong (electron) beam is increased in steps. Bunch lifetime becomes short in positron train 3, bunch 1 when the electron bunch currents reach 4 mA. In this measurement a perturbing electron beam with 4 bunches in train #1 disrupted a positron test beam with trains #2-9 filled with 4 bunches each.

The primary limitations are a poorly tuned interaction region where the 1 Tesla experiment solenoid field is compensated by a several pairs of skew quads, and the effects of parasitic beam-beam interactions. The future commissioning plan focuses on improving our understanding of the interaction region optics and doubling the damping rate with six more wigglers.

6. ACKNOWLEDGEMENTS

These accomplishments are the result of the dedicated and capable work of the entire LEPP staff. The data presented herein was acquired, analyzed, and presented by the CESR operations group members. Figure 1 is from J. Crittenden, and figures 3-6 are from A.B. Temnykh.

The work described here was performed under a contract with the U.S. National Science Foundation

References

- [1] D. Rice, *Proc. EPAC 1996*, p. 17
- [2] D.L. Rubin et al., *Proc. PAC 2001*, p. 3520
- [3] R. Littauer, *IEEE NS-32*, p. 1610 (1985)
- [4] <http://www.lns.cornell.edu/public/CLEO/spoke/CLEOc/ProjDesc.html>
- [5] J. Corbett, Y Nosochkov, *Proc. PAC 1999*, p. 2358
- [6] J. Safranek et al., *Proc. EPAC 2000*, p. 295
- [7] J. Crittenden et al., *Proc. PAC 2003*, p. 1954
- [8] D. Rice, *Proc. PAC 2003*, p. 167
- [9] D. Sagan CESR lattice design in ICFA Beam Dynamics Panel Newsletter No. 31 <http://wwwslap.cern.ch/icfa/>